Carboxy Mb at pH 3

Time-resolved resonance Raman study at cryogenic temperatures

I. E. T. Iben,*‡ B. R. Cowen,§ R. Sanches,‖ and J. M. Friedman*‡

*AT&T Bell Laboratories, Murray Hill, New Jersey 07974; Chemistry Department, ‡New York University, New York 10003; §Physics Department, University of Illinois at Urbana-Champaign, Champaign, Illinois 61801 USA; and ‖Physics Department, University of Sao Paulo, Sao Paulo, Brazil

ABSTRACT Cryogenic samples of MbCO at pH3 are studied using nanosecond and picosecond time-resolved resonance Raman spectroscopy. It is observed that under excitation conditions sufficient to completely photodissociate MbCO at pH7, the pH3 sample at 10 ns remains substantially unphotolyzed even at 15 K. The similarity in the optical and resonance Raman spectra of MbCO at pH3 with that of pH7 indicates that at pH3 the iron remains six-coordinate and low-spin. The Fe-CO stretch frequency is consistent with a more upright CO orientation. The absence of the ν(Fe-His) band in the 30 ps photoproduct Raman spectrum suggests that the Fe-His(F8) bond is broken within 30 ps of photodissociation. Other Raman bands, though, are not consistent with a normal four-coordinate heme for the photoproduct, Mb*. Suggested possible interpretations include a four-coordinate heme highly perturbed by the close lying protonated proximal histidine or a five-coordinate heme with the Fe-His bond significantly weakened. The partial photolysis monitored at 30 ps and 100 K indicates either a significant amount of geminate recombination within 30 ps or a low quantum yield for photolysis. The time course for CO recombination is monitored via the Raman spectra from 30 ps to 3 ns at 100 K and 160 K. Of the fraction of protein-ligand pairs that remain photodissociated at 30 ps, 50% recombine by ~250 ps at 100 K and 160 K, supporting the flash photolysis rebinding data of Cowen et al. (Cowen, B. R. 1990. Ph. D. thesis. University of Illinois at Urbana-Champaign; Cowen, B. R., D. Braunstein, H. Frauenfelder, P. J. Steinbach, and R. D. Young. 1989. *Biophys. J.* 55:55a. [Abstr.].) The conclusions from these resonance Raman studies are extended to solution phase studies at ambient temperatures.

INTRODUCTION

The interaction of the proximal histidine with the heme is thought to be a source of control for ligand binding kinetics in heme proteins. Such interactions are grouped under the term of proximal restraint. Attempts to expose and control proximal effects in ligand binding studies have included model heme compounds (1–4). A solution of carbonmonoxy protoheme in the absence of a strong sixth ligand is thought to be a good model system for studying ligand binding effects in the absence of proximal influences. Flash photolysis experiments on protoheme have recorded CO rebinding rates that are greatly enhanced (1–3) compared with those measured for Mb at pH7 (5). Such studies are limited because the heme environment in model compounds is radically different from that found in proteins. Rebinding studies of CO to Mb at pH 2.6 and 300 K reveal a 40-fold increase in the CO binding rate that is associated with a protein protonation with a pK of ~3.45 (6, 7). Low temperature rebinding dynamics measured by flash photolysis methods yield rebinding kinetics for MbCO at pH3 (8, 9) that are similar to those measured for protoheme (1–3), though differences between the two systems are discernable. Fast kinetics and optical absorption studies have lead to the suggestion that under these low pH conditions the covalent bond between the iron and the proximal histidine, Fe-His bond, is broken. This conclusion raises the possibility of using low pH Mb as a protein model for ligand rebinding in the absence of proximal restraint.

Resonance Raman spectroscopy offers a more detailed structural picture of the heme and its environment than does absorption spectroscopy. Resonance Raman bands of hemes have been well characterized, yielding information on the spin, coordination, and environment of the heme (10). Han et al. (11) obtained-resonance Raman spectra of deoxy and carboxy Mb after rapid drops in pH at ambient temperatures. Their results indicate that MbCO in water at pH 2.6 is a six-coordinate, low-spin species. The limited but discernable differences between the resonance Raman spectra of MbCO at pH 2.6 and pH 7 indicate a more open distal pocket with the CO in a more upright orientation in the former. The changes in the structure at the heme upon dropping the pH to 2.6 appear to be much more substantial for deoxy Mb at pH3 than for MbCO. The resonance Raman spectrum of deoxy Mb suggests that the Fe-His bond is broken. However, the spectra were also interpreted to indicate that the heme is five-coordinate with a water molecule as the probable weak

Address correspondence to Dr. Friedman.

0006-3495/91/04/908/12 $2.00

fifth ligand. This study did not examine the time scale or sequence of events that are associated with the evolution of a six-coordinate MbCO species to a protoheme like species upon photodissociation. This information is crucial because if the breakage of the Fe-His bond is fast compared with subsequent recombination, then this system is a potentially useful model for separating proximal and distal influences on the recombination kinetics. The present study addresses these issues.

In this paper we report the resonance Raman spectra of MbCO and its photoproduct, Mb*, at pH 3 under the same cryogenic conditions as employed in the transient absorption studies of Cowen et al. (8, 9). Time-resolved resonance Raman spectra with 30 ps resolution yield recombination kinetics that are similar to those measured by Cowen et al. (8, 9) using transient absorption spectroscopy. The structure local to the heme of MbCO at pH 3 probed at cryogenic temperatures remains essentially the same as observed at room temperature. The Fe-His bond appears to rupture within 30 ps of photodissociation. However, as observed in room temperature measurements (11), other parts of the spectra are not consistent with a conventional four-coordinate species. We offer several possible mechanisms to account for the unusual spectra. An extension of this analysis to room temperature conditions with a comparison to several room temperature studies (11, 12) is presented.

MATERIALS AND METHODS

The preparation of stable Mb at low pH is difficult. At pH ≤ 3, both deoxy and carboxy Mb denature in water at room temperature in the millisecond time range (7, 8, 11). The pK for the denaturation of deoxy Mb is ~3.5 (7), with a lower value for MbCO. The presence of glycerol serves to stabilize MbCO in its folded structure (8). We have found that in the absence of O_2, MbCO at pH 3 is stable for several days at room temperature in both 25 and 75% glycerol/water solvents. This stability is verified by measuring the optical absorption of the samples both before and subsequent to performing the resonance Raman experiments. The absorption spectra of MbCO at pH ≤ 3 is similar to that measured at pH7 (8, 11). The alpha and beta bands are at essentially the same positions as for pH 7, but the relative amplitudes are adjusted slightly. The Soret blue shifts only 1–3 nm to between 420 and 423 nm and maintains a half width of ~25 nm. Protoheme-CO also maintains a half width of ~25 nm, but is at ~411 nm (1). Furthermore, protoheme does not remain in solution except at alkaline pH. The spectra are also not characteristic of denatured Mb, for which the Soret broadens and shifts to: ~400 nm (full width at half maximum of ~25 nm) for MbCO, ~390 nm (fwhm of ~100 nm) for met-Mb (13), and ~390 (fwhm of ~100 nm) for deoxy-Mb (7). Thus the MbCO samples at pH 3 in both 25 and 75% glycerol/water appears to remain six-coordinate with the globin folded about the heme.

Sperm whale myoglobin, Mb, was purchased from Sigma Chemical Co. (Saint Louis, MO). Powdered Mb (17 mg) was dissolved in 0.5 ml of a 90% glycerol/water mixture. This solution was alternatively degassed and CO saturated several times during a 24-h period. Sodium dithionite ($Na_2S_2O_4$) (6 ul, 1 M) was added to the mixture to reduce the Mb, which was again CO saturated and stirred for another hour to ensure a complete MbCO mixture. At this point 0.1 ml of potassium phosphate buffer (1.5 M, pH 2.6) was added to the mixture, resulting in a protein concentration of ~2 mM and a pH of 3. The sample was then loaded in an air-tight sample cell having a 0.25-mm thick mylar spacer sandwiched between two sapphire windows. The visible absorption was then measured to ensure the sample integrity. In cases where the sample was not fully CO bound, the samples denatured within several seconds and a new sample was prepared. The sample was then loaded in a continuous flow cryostat (R. G. Hansen and Associates, Santa Barbara, CA) and the temperature was immediately lowered to 250 K or below. When the experiment was complete, the absorption spectrum was checked to ensure that the sample has remained intact.

For the nanosecond studies, a Lambda Physik (Götingen, Germany) excimer pumped (~10 ns fwhm) (EMG 101) tunable dye laser (2002) was used for both photodissociation and simultaneous generation of the resonance Raman scattering. The output of the dye laser (tuned between 423 and 430 nm, stilbene 3) was ~10 mW at 10 Hz with a pulse duration of ~10 ns. The laser pulse passed through a prism assembly to remove amplified stimulated emission. A 20-cm focal length cylindrical lens was used to produce a line focus to avoid burning the sample. This beam is focused onto the front surface of the sample to an area of ~10 mm by 0.5 mm.

For the picosecond time-resolved measurements, the samples were photolyzed by 532 nm, ~30 ps pulses (~3 mJ/pulse) from the second harmonic of a 10-Hz active-passive mode-locked Nd-YAG laser (Quantel). The samples were then probed with 435.7 nm, ~30 ps pulses created by the anti-Stokes shifted 532 nm light that was passed through a Hydrogen filled (~300 psi) Raman shifter. To minimize photolysis by the probe beam for the time-resolved measurements, the 435.7 nm light was attenuated to ~20 μJ/pulse. A time differential of up to 10 ns was obtained by passing the 532 nm light along variable lengths of a 1-m long double pass delay stage (Klinger). A cylindrical lens was used to focus the beams onto the sample to avoid sample damage. The areas of the 435.7 and the 532 nm pulses were ~10 by 1 mm and 20 by 3 mm, respectively, so that the latter overfilled the former.

For all of the resonance Raman data, a back scattering geometry with ~45° between the laser k vector and the optical axis of the spectrometer was used. The scattered light was collected by a two lens assembly and sent through a double monochrometer (U1000; Instruments SA, Metuchen, NJ) using either 2,400 or 600 g/mm matched gratings. The dispersed light was then collected by an intensified Optical Multichannel Analyzer (OMA) (IRY with 1024 diodes, ~500 of which are intensified; Princeton Instruments, Princeton, NJ.). A Princeton Instruments controller (ST-110) and an AT&T 640 PC were used for communications. The instrument resolution was ~2 and 7 cm^{-1} for the 2,400 g/mm and 600 g/mm gratings, respectively.

RESULTS

Figs. 1, *a–d* show high resolution resonance Raman spectra of the porphyrin breathing mode ν_4[1] (14, 15) for MbCO at pH 7 and pH 3 at cryogenic temperatures with 10 ns (1 mJ/pulse, 10 Hz) laser pulses with excitation wavelengths, λ_{exc}, of 430 and 423 nm. The frequency of ν_4 is sensitive to the oxidation, spin, and ligation state of the heme (15–18). The high and low frequency ν_4 bands seen in Fig. 1 are due to the liganded and photodissoci-

[1]All assignments are from Abe et al. (14).

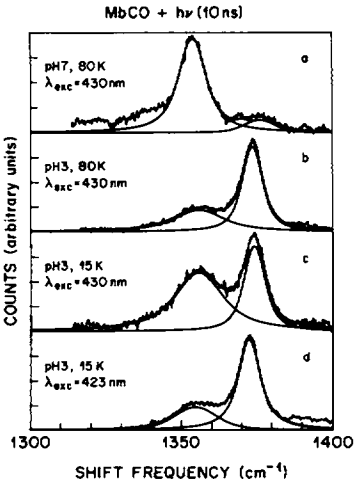

FIGURE 1 Resonance Raman spectra of ν_4 for a mixture of MbCO and Mb*(10 ns) in 75% glycerol/H_2O. The pump-probe pulses were from a 10-Hz excimer pumped dye laser with a temporal width of 10 ns fwhm and an average power of ~10 mW. The gratings, slit width, and accumulation time were: 2,400 g/mm, 420 μ, and 5 min: (*a*) pH 7, 80 K, λ_{exc} = 430 nm; (*b*) pH 3, 15 K, λ_{exc} = 430 nm; (*c*) pH 3, 80 K, λ_{exc} = 430 nm; (*d*) pH 3, 15 K, λ_{exc} = 423 nm. The fits are explained in the text.

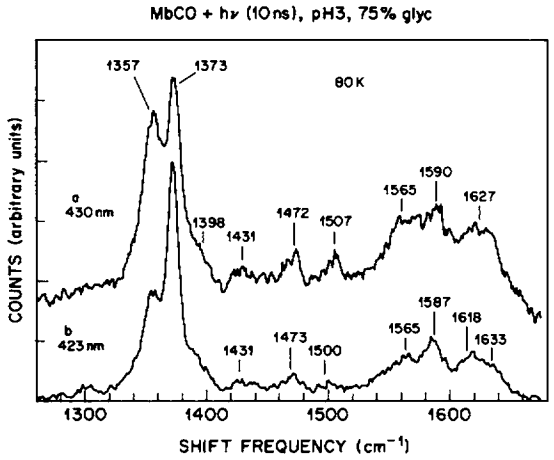

FIGURE 2 Resonance Raman spectra for the high frequency region for a mixture of MbCO and Mb*(10 ns) in 75% glycerol/H_2O at pH 3 and 80 K. The pump-probe pulses were from a 10-Hz excimer pumped dye laser with a temporal width of 10 ns fwhm and an averge power of ~10 mW. The gratings, slit width, and accumulation time were: 600 g/mm, 22 μ, and 30 min: (*a*) λ_{exc} = 430 nm; (*b*) λ_{exc} = 423 nm.

ated species, respectively. The two ν_4 bands are fit by two voigtians (20) (gaussian convolutions of lorentzians) centered at ~1,374 and ~1,356 cm^{-1}. A linear background is subtracted off. The fit to the 1,374 cm^{-1} band, which we attribute to MbCO, has a full width at half maximum, fwhm, of ~8.5 cm^{-1} for both pHs. The 1,356 cm^{-1} band, which we attribute to Mb*, has a fwhm of ~19 cm^{-1} for the pH 3 samples, and ~ 12 cm^{-1} for the pH 7 sample. Fig. 1 *a* shows ν_4 for pH 7 MbCO at 80 K and λ_{exc} = 430 nm. The ratio in integrated area of the 1,356 cm^{-1} peak (A_d) compared with the 1,374 cm^{-1} peak (A_b) is: $R_{db} = A_d/A_b \sim 9$. In comparison, $R_{db} \sim 0.6$ for the pH 3 sample under the same conditions, (Fig. 1 *b*) (though the intensity ratio is only ~0.3, the increased width of ν_4[1,356] compared with the width of ν_4[1,374] leads to the higher ratio of R_{db}). Figs. 1, *c* and *d*, respectively, show ν_4 for pH 3 MbCO at 15 K with 10-ns pulses of λ_{exc} = 430 nm (R_{db} ~ 1.6) and λ_{exc} = 423 nm (R_{db} ~ 0.6).

Figs. 2, *a–b* show high frequency spectra from 1,250 to 1,700 cm^{-1} for pH 3 MbCO at 80 K photolyzed and probed with 10-ns pulses at λ_{exc} = 430 nm (Fig. 2 *a*) and λ_{exc} = 423 nm (Fig. 2 *b*), (~1 mJ/pulse, 10 Hz). The most intense band is ν_4, which for both excitations is split with peaks at ~1,356 and ~1,374 cm^{-1}. The value of R_{db} is ~0.9 with λ_{exc} = 430 nm (Fig. 2 *a*), and ~0.3 with λ_{exc} = 423 nm (Fig. 2 *b*). Other less prominent bands with intensities between ~10 and 20% of ν_4(1,374) are seen at higher frequencies. Using λ_{exc} = 430 nm, peaks are seen at 1,431, 1,472 (ν_3), 1,507 (ν_3), 1,565 (ν_2), 1,590 (ν_2), and 1,627 cm^{-1} (ν_{10}). With λ_{exc} = 423 nm, peaks are seen at 1,431, 1,473 (ν_3), 1,500 (ν_3), 1,565 (ν_2), 1,587 (ν_2), 1,618 (ν_{10}), and 1,633 cm^{-1} (ν_{10}).

Figs. 3, *a–d* show the low frequency spectra taken under conditions identical to those for the corresponding ν_4 in Figs. 1, *a–d*. The Fe-proximal histidine stretching mode is a Raman band which is important for determining the coordination of the Fe. The Raman band is found between 216 and 242 cm^{-1} for five coordinate high spin heme proteins (16–21). Fig. 3 *a* is of pH 7 MbCO at 80 K with λ_{exc} = 430 nm. The most intense protein band in this range is ν(Fe-His) at 231 cm^{-1}. The other observed bands are at 246, 269, 304, 345 (ν_8) (14) and 371 cm^{-1}. The relative intensities of these bands with respect to that of ν(Fe-His) are ~0.7, 0.2, 0.25, 0.3, and 0.3. Figs. 3, *b* and *c* are, respectively, the 80 and 15 K resonance Raman spectra of pH 3 MbCO photoexcited and probed with λ_{exc} = 430 nm. The intensities are normalized so that A_d of the corresponding 1,356 cm^{-1} band matches A_d for the pH 7 sample, Fig. 1 *a*. The dominant band is ν_8 at ~351 cm^{-1}, having an intensity approximately equal to that of ν(Fe-His) at pH 7. Three other bands are observed at 234, 367, and 304 cm^{-1}. The intensities of these bands are ~25% that of the ν(Fe-His) band and equal to that of the 304 cm^{-1} band for the pH 7 spectrum (Fig. 3 *a*). With λ_{exc} = 423 nm (Fig. 3 *d*), no bands are observed in the proximity of 231 or 304 cm^{-1}. The two bands seen are at 267 and 351 cm^{-1}.

Another important band for determining the ligation

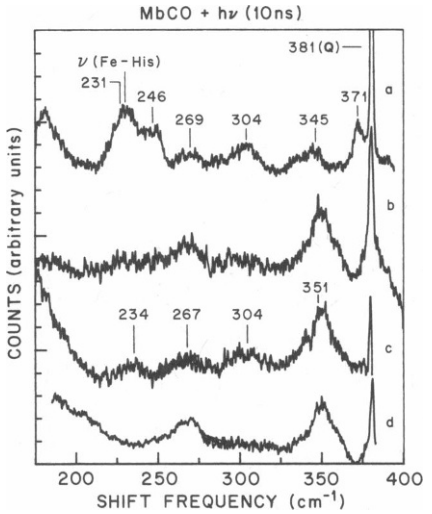

FIGURE 3 Resonance Raman spectra of the low frequency range for a mixture of MbCO and Mb*(10 ns) in 75% glycerol/H_2O. The pump-probe pulses were from a 10-Hz excimer pumped dye laser with a temporal width of 10 ns fwhm and an averge power of ~10 mW. The gratings, slit width, and accumulation time were: 2,400 g/mm, 420 μ, and 5 min.: all data are normalized so that the integrated area for the corresponding ν_4(1,356 cm^{-1}) match that for the pH 7 sample (Fig. 1): (*a*) pH 7, 80 K, λ_{exc} = 430 nm. ν(Fe-His) ~ 231 cm^{-1}; (*b*) pH 3, 15 K, λ_{exc} = 430 nm; (*c*) pH 3, 80 K, λ_{exc} = 430 nm; (*d*) pH 3, 15 K, λ_{exc} = 423 nm.

state of Mb is the Fe-CO stretch, ν(Fe-CO). Fig. 4 shows the resonance Raman spectrum between 425 and 535 cm^{-1} for pH 3 MbCO excited and probed with λ_{exc} = 423 nm at 15 K. The peak at ~495 cm^{-1} with a shoulder at 481 cm^{-1} is ν(Fe-CO). The intensity of ν(Fe-CO) is 25%

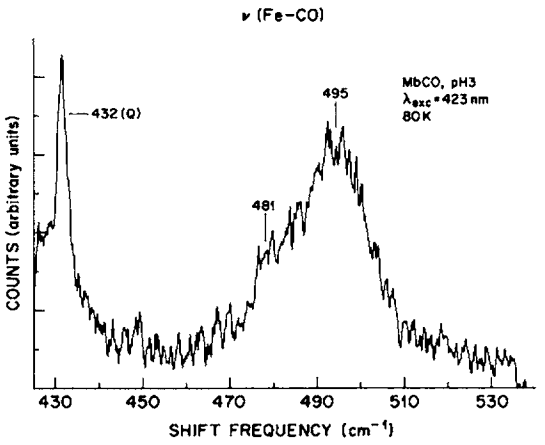

FIGURE 4 Resonance Raman spectra of ν(Fe-CO) for MbCO at pH 3 in 75% glycerol/H_2O at 80 K. λ_{exc} = 423 nm (10 ns) power = 10 mW. The gratings, slit width, and accumulation time were: 2,400 g/mm, 420 μ, and 5 min.

the intensity of ν_7 (14) at ~676 cm^{-1} (not shown). Furthermore, no bands are observed at either ~507 or ~531 cm^{-1}.

Figs. 5, *a–b* are low frequency resonance Raman spectra of MbCO samples at both pH 7 and pH 3 at 100 K photodissociated by 30 ps pulses at 532 nm (3 mJ) and probed with temporally overlapping 435.7 nm (80 μJ) pulses (10 Hz) (Figs. 5 *a–b*). The spectrum for pH 7 (Fig. 5 *a*) contains three bands at 228, 242, and 267 cm^{-1} with relative intensities of 1 to 0.7 to 0.1. The fits are voigtians with their shapes all set equal. As discussed earlier, the 228 cm^{-1} band is associated with ν(Fe-His). To compare the data for the two pH's, the resonance enhancement of the ν(Fe-His) band relative to that of the ν_4(1,356) band is taken to be the same for the two pH's. Thus, the low frequency pH 3 spectra are normalized so that the associated A_d matches that of the pH 7 sample. Two bands are seen in the pH 3 spectrum at ~304 and ~351 cm^{-1} with peak heights having signal to noise (*S/N*) levels of 1 to 1. No clear band is seen in the spectral range associated with ν(Fe-His), with the magnitude of the noise being 25% (peak-to-peak) of the expected height of ν(Fe-His) based on the pH 7 spectrum.

The time dependence of ν_4 was also measured from 30 ps to 3 ns at 100 and 160 K for Mb at pH 3. Fig. 6 shows the time evolution of ν_4 probed with 30-ps pulses at 435.7 nm taken at the overlap time of 15 ps (±15 ps), at 600 ps after and 60 ps before the 530 nm excitation pulse. The

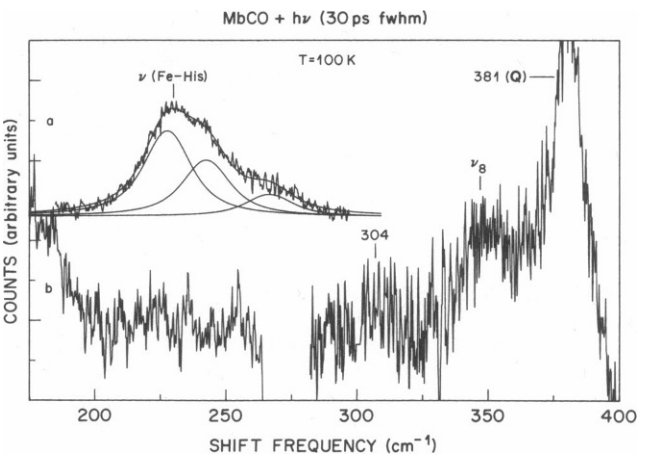

FIGURE 5 Resonance Raman spectra of the Fe-His region at 80 K for the 30 ps photoproduct of MbCO at 100 K: (*a*) pH 7: the data is fit with three bands at 228, 241, and 267 cm^{-1}; (*b*) pH 3: the data is from two wavelength settings of the spectrometer that did not overlap, hence the missing segment at ~275 cm^{-1}. The data are normalized so that the integrated area of ν_4(1,356 cm^{-1}) are matched. 2,400 g/mm gratings and an entrance slit of 420 μ were used for both sets, with accumulation times of 5 min for *a* and 30 min for *b*.

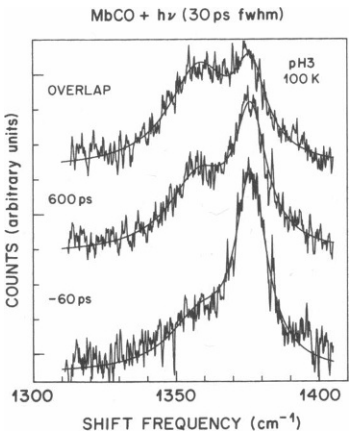

FIGURE 6 Transient resonance Raman spectra of partially photolyzed MbCO in 75% glycerol/H_2O at pH 3, 100 K. Three delay times between the excitation (530 nm, 30 ps, 30 mW) and the probe pulse (435.7 nm, 30 ps, 0.2 mW) are shown: (*a*) overlap; (*b*) 600 ps; (*c*) −60 ps. 2,400 g/mm gratings and an entrance slit of 420 μ was used. The data are each the sum of two 30 min acquisitions. The fits (*smooth curves*) are with a lorentzian with peak at 1,374 cm^{-1} and fwhm of 12 cm^{-1}, and a gaussian with peak at 1,356 cm^{-1} and fwhm of 29 cm^{-1}.

data is also fit to a lorentzian for the 1,373 cm^{-1} peak and a gaussian for the 1,356 cm^{-1} peak. The shape and peak of the gaussian for ν_4(1,356) is determined by fitting the difference between the overlap time and the infinite time spectrum to a gaussian. The resulting fwhm of 25 cm^{-1} and peak position of 1,356 cm^{-1} are then held fixed and the infinite time data is fit by adding a lorentzian, whose fwhm and peak position are found to be 12 and 1,376 cm^{-1}. The remaining spectra are then fit keeping the widths and peak positions of these bands fixed. Table 1 gives the values of R_{db} for various times at 100 and 160 K.

DISCUSSION

Carbonmonoxy myoglobin

The similarity in the Soret spectrum of MbCO at pH 3 to the spectrum of MbCO at pH 7 rather than to protoheme or a denatured protein indicates an intact, six-coordinate low spin species with the proximal histidine still bound to the heme. The resonance Raman spectra at ambient (11) and cryogenic temperatures corroborate this assignment, and in addition, specify a more open protein structure. As stated earlier, ν_4 is sensitive to the ligation state of the heme. For four- and six-coordinate species with the iron in the heme plane, ν_4 is found between 1,370 and 1,380 cm^{-1} (15–17). For five-coordinate, high spin hemes with the iron out of the mean heme plane, ν_4 shifts to ~1,356 cm^{-1} (16–18). Since with λ_{exc} = 423 nm, ν_4 is predominantly 1,374 cm^{-1} at 80 K, (R_{db} ~ 0.20), either a predominantly four- or six-coordinate species is probed in this situation. Except for a broadening and blue shifting of the vinyl ν_{10} (15), the remainder of the high frequency spectrum matches that of pH 7 MbCO at 300 K (11). The blue shift is attributed to an "opening" up of the heme environment based on comparisons to 2-Melm-protoheme at 300 K (11).

Further indication of a six-coordinate heme for MbCO comes from the ν(FE-CO) band. Both a five-coordinate MbCO species and a six-coordinate MbCO species with a weak axial ligand can be ruled out because no bands representative of ν(Fe-CO) are observed between 526 and 531 cm^{-1} (22). The shift in the position of ν(Fe-CO) from 507 cm^{-1} for pH 7 to ~495 cm^{-1} with a shoulder at ~481 cm^{-1} for pH 3 is indicative of a six-coordinate heme with the CO in a more upright orientation associated with an open pocket (11, 23, 24). This effect, though, is associated with a pK between ~3.8 (23) and ~4.4 (24), and is probably caused by the protonation of the distal histidine (His-E7). The intensity of the ν(Fe-CO) band measured at 15 K using λ_{exc} = 423 nm is ~25% of the intensity of ν_7(~676), and ~12% of the intensity of ν(~1,376). These ratios are approximately the same as measured for MbCO at 300 K and pH 7 (23). Thus, the ν_4(~1,376) measured in these experiments is predominantly associated with six-coordinate MbCO species.

Photoproduct, Mb*

The photoproduct spectra display a broad band at 1,356 cm^{-1}. Such a position for ν_4 is usually associated with a five-coordinate, high spin species with the Fe^{2+} out of the porphyrin plane (16, 18). A significant contribution to ν_4 at 1,374 cm^{-1} still remains which, as discussed above, is attributed to MbCO. The remainder of the high frequency spectrum is consistent with an admixture of five- and six-coordinate hemes. While 430 nm excita-

TABLE 1

Delay time	0 *ps*	20 *ps*	50 *ps*	100 *ps*	300 *ps*	600 *ps*	900 *ps*	3 *ns*	−60 *ps*
R_{db} (100 *K*)	2.4	2.5	1.9	1.5	—	—	1.1	0.92	0.54
R_{db} (160 *K*)	3.0	—	—	1.7	1.6	—	1.0	—	0.71

tion leads to an enhancement of Mb*, 423 nm excitation leads to an enhancement of the MbCO spectrum. Thus Mb* cannot be unambigously determined because of the substantial contributions from MbCO in the resonance Raman spectrum with λ_{exc} = 430 nm. In addition, both the insufficient S/N and the fact that the relative resonance Raman enhancement of the various bands is wavelength dependent (25), which makes it difficult to use the difference spectrum from the two excitation wavelengths to generate a reliable Mb* spectrum. The absence of a band at 1,521 cm^{-1}, though, is indicative of a broken Fe-His bond (11), while the position of ν_{10} at ~1,627 cm^{-1} is indicative of a five-coordinate rather than a four-coordinate heme (17).

The low frequency resonance Raman spectrum contains direct evidence concerning the state of the Fe-His bond. The low frequency spectrum of pH 7 Mb at 80 K with λ_{exc} = 430 nm represents five-coordinate Mb*, which is consistent with the predominance of a ν_4 at 1,356 cm^{-1}. The dominant band at 231 cm^{-1} is associated with ν(Fe-His) (16, 26). Both ν(Fe-His) and the 304 cm^{-1} bands are present in the spectrum of Mb* and not in the spectrum of MbCO. These and the other observed bands are in the positions described in previous studies of Mb* at pH 7 and 80 K (16). Assuming that the λ_{exc} = 430 nm the ratio of resonance Raman cross-sections of the low frequency bands to ν_4(1,356) are about the same at pH 3 as at pH 7, a comparison of Mb* for the two pH's can be made (Fig. 3, *a–c*). The 304 cm^{-1} band present in the pH 3 spectrum at 15 K, Fig. 3 *c*, has about the same intensity relative to ν_4 as in the pH 7 spectrum, Fig. 3 *a*, while its intensity at pH 3 and 80 K, Fig. 3 *b*, is only half as intense. The weak band at 234 cm^{-1} seen in the pH 3 samples is possibly ν(Fe-His). Its relative intensity, though, is at most 25% that measured for the pH 7 sample. These data indicate that at most 25% of the proteins photodissociated at 15 or 80 K that are associated with ν_4(1,356) retain the Fe-His bond. A comparison of low frequency spectra on a 30-ps time scale, Figs. 5, *a* and *b*, also reveal the absence of ν(Fe-His) for the pH 3 sample, with the S/N giving an upper limit up to the intensity of ν(Fe-His) of 25% that measured at pH 7. Since with a pK of ~3.5 (7), 25% of the proteins should remain unprotonated at pH 3, this data is consistent with the protonated molecules having an altered Fe-His linkage that results in ν(Fe-His) not being detected.

If the Fe-His bond is broken within 30 ps of photodissociation, then it is reasonable to assume that the photoproduct, Mb*, at pH 3 would contain a four-coordinate heme. A planar four-coordinate heme should be intermediate spin with a ν_4 of ~1,374 cm^{-1} (15, 17). The spectra of pH 3 samples of Mb* at cryogenic (this report) and deoxy Mb (11) at ambient temperatures both reveal a ν_4 band at ~1,356 cm^{-1}. This frequency is normally associated with five-coordinate, high spin ferrous porphyrins (16, 18). Given the alleged rupture of the Fe-His bond, the question arises as to the origin of the spectral feature that implies a five-coordinate heme. As discussed earlier, the ν(Fe-CO) spectral region of the Mb*-MbCO cryogenic mixture rules out the presence of a five-coordinate carbonmonoxy heme species because of the absence of a band at ~531 cm^{-1} (22). Han et al. (11) suggest that the presence of ν_4 at ~1,355 cm^{-1} for deoxy Mb after a rapid drop in pH to ~2.6 at room temperature, is likely to be due to water as a fifth ligand. This suggestion is reasonable since the loosening of the protein under these denaturant conditions could allow for easy access of a water molecule into the proximal heme pocket subsequent to the rupture of the Fe-His bond. It is, however, difficult to envision a similar mechanism being responsible for the same ν_4 value in the 30 ps or 10 ns photoproduct spectrum at cryogenic temperatures; consequently, we consider causes other than a bound water to account for the five-coordinate like value of ν_4.

The frequency of ν_4 is sensitive to the extent of π electron back donation by the iron ion to the porphyrin marocycle (16–18). It has been shown (15, 18) that planar four-coordinate ferrous porphyrins with an intermediate spin have a ν_4 frequency similar to that of both ferric and ferrous low spin forms (both having three d_π electrons) (27). In the heme protein example at hand, there are distinct molecular differences compared with the solution phase model compound studies that yielded the above conclusions regarding ν_4. These differences could in principle produce a four-coordinate species with an atypical ν_4 frequency.

If the dissociated protonated proximal histidine were constrained to be in close proximity to the heme, then the structure and electronic properties of the heme might be perturbed. Evidence for such structural constraints come from femtosecond transient absorption studies of T-state NOHb. T-state NOHb has α subunits that are five-coordinate due to breakage of the Fe-His bond (28, 29). The femtosecond photolysis studies of Martin and co-workers (30) on T-state NoHb show that upon photodissociating the NO-heme complex, a five-coordinate deoxy like heme spectrum is formed within 300 fs. This result indicates that the unbound proximal histidine is constrained to a position close to the four-coordinate heme. We believe it plausible that in our case as well, the proximal histidine is constrained to be in close proximity to the heme both at cryogenic and, at least transiently, at ambient temperatures.

A protonated proximal histidine in close proximity to a four-coordinate heme could influence ν_4 in any of several ways that could perturb the π back bonding between the iron and the porphyrin macrocycle. Clearly

a proton on the N_ϵ of the imidazole ring could have a direct inductive effect on the charge distribution in the porphyrin ring if it were close enough. Another possibility is that the close proximity of the protonated N_ϵ of F8 to the heme iron results in a sufficient coulombic repulsion to stabilize a nonplanar four-coordinate heme which changes the iron from intermediate to high spin. In a homogeneous dielectric medium (dielectric constant = ϵ), the change in electrostatic potential energy associated with moving the Fe^{2+} out of the porphyrin plane away from a proton situated a distance R from the heme plane is, to lowest order, given by:

$$V(p) = -\frac{pe}{\epsilon R^2}. \quad (3)$$

Where p is the change in the dipole moment of the heme. The equilibrium configuration for a four-coordinate heme is with the Fe^{2+} in the porphyrin plane, so that moving the Fe^{2+} a distance d out of the porphyrin plane costs energy. Assuming this potential to be harmonic with a force constant k, and with p being linear with d ($q_{eff} = p/d$), minimizing the energy with respect to d results in a displacement of the Fe^{2+} by:

$$d = 2R_\infty \frac{q_{eff}}{\epsilon R^2}\left(\frac{a_0}{k}\right) \quad (4)$$

a_0 ($\sim$0.5 Å) is the Bohr radius and R_∞ is the Rydberg constant (= 13.6 eV). Assuming ϵ is between 2.5 and 4 (31), R is between 2.2 and 2.7 Å,[2] q_{eff} is between 0.22 and 0.35 (32), and with k between 1 and 2 eVÅ^{-2} (33, 34) the resulting value of d is between 0.04 and 0.4 Å, which is comparable to the 0.3 to 0.5 Å distance the Fe^{2+} lies out of the mean heme plane for five-coordinate deoxy hemes (35–38). The broadness of ν_4(1,356) could then be interpreted as a distribution in iron out-of-plane distances resulting from a distribution in R.

In the resulting picture, an obvious unanswered question is by what mechanism does the six-coordinate CO bound heme evolve into the proposed four-coordinate species upon photodissociation. The appearance within 30 ps of a perturbed photoproduct spectrum in the cryogenic sample indicates that the MbCO sample is already protonated before photolysis. The similarity of this spectrum to the room temperature spectrum indicates an absence of pumping effects due to repetitive pulsing. The presence of a six-coordinate CO species strongly indicates, however, that the N_ϵ of F8 is not protonated. If one assumes that a protonated N_ϵ is responsible for the Fe-His bond rupture, it is necessary to invoke a mechanism whereby a proton shifts to N_ϵ within 30 ps of photolysis. One possibility is that the additional proton is on N_δ. N_δ is normally hydrogen bonded to a backbone carbonyl the protein. The added proton on N_δ might also alter the strength of this hydrogen bond. Upon photolysis, the proton would then undergo rapid shifting to N_ϵ and the hydrogen bond between the F-Helix and N_δ would resume its original strength.

An alternate possibility is that the iron remains coordinated to the proximal histidine both in the ligand bound and dissociated species but with the Fe-His linkage altered in a way that makes its detection difficult even for the five-coordinate species. For ν(Fe-His), either a loss in the relative resonance enhancement or a substantial decrease in frequency could account for the absence of a clearly discernable Raman band. It has been shown (39) that the Fe-His bond strength, as reflected in the frequency of ν(Fe-His), is highly responsive to the status of the proton of N_δ. The progressive loss of the proton on N_δ results in an increase in the Fe-His bond strength. In a study (39) on 2-methylimidazole (2-MeImH) bound to Fe^{2+} model porphyrins, ν(Fe-His) shifted from 205 cm^{-1} in benzene to 220 cm^{-1} in water due to increased hydrogen bonding of the imidazole proton to water. A further upward shift in ν(Fe-His) to a 239 cm^{-1} is observed when the imidazole proton is fully removed in the presence of a strong base. Similarly, in cytochrome c peroxidase (CCP), where the hydrogen bond is much stronger than in Mb due to the carboxyl group of Asp 235, the frequency of ν(Fe-His) is shifted to a much higher frequency (240 cm^{-1} vis-a-vis 220 cm^{-1}) (40). Replacement of Asp 235 in CCP with an Asn, (41) which does not have the proton accepting capability of Asp results in a shift of ν(Fe-His) down to 205 cm^{-1}. These results are consistent with the idea that the degree of protonation at N_δ modulates the shifting of electron density between the Fe-His bond and the imidazole macrocycle.

The addition of a second proton at N_δ, as we are suggesting for Mb at low pH, should produce a more exaggerated effect than either the Asp 235 → Asn substitution discussed above for CCP or the absence of hydrogen bonding for model systems in nonhydrogen bonding solvents. The N_δ now has both a proton involved in a moderate H-bond with a backbone carbonyl and an additional pH-derived proton. The double proton arrangement could be stabilized by a substantial shift of electron density toward N_δ at the expense of the Fe-His bond above and beyond what occurs in just the abscence of hydrogen bonding. Thus, a frequency below 205 cm^{-1} would not be unreasonable based on both the CCP and

[2]The N_ϵ of the proximal Histidine is assumed to be protonated (6, 7). When coordinated to the iron, the N_ϵ-Fe^{2+} distance is $\sim$2.2 Å (21). Assuming that the proton coordinated to N_ϵ lies between this distance and 0.5 Å further away from the mean heme plane, then R is between 2.2 and 2.7 Å.

the model compound results. Furthermore, a shift of electron density from the vicinity of the iron into the imidazole ring could also decrease the resonance enhancement for ν(Fe-His) because of reduced overlap in the π systems.

If the added proton at N_δ substantially weakens the Fe-His bond through electronic effects as opposed to the structural factors that are alleged to occur in hemoglobin (16, 42), then the associated lengthening of the Fe-His bond could result in a more in-plane iron. A weakened and lengthened Fe-His bond with a more in-plane iron would be expected to yield a reduced barrier for the formation of an iron-ligand bond. Erythrocruorin from Chironomus thummi thummi binds CO with a very high rate ($k = 2.7 \times 10^7$ M^{-1} s^{-1}) (43). This heme protein shows the same low pH-induced changes in the optical spectra that occur for other hemeproteins, but does not display a further increase in reactivity (6). The x-ray derived structure for deoxyerythrocruorin at pH 7 reveals a pentacoordinate iron (Fe^{2+}) but with the iron much closer to the heme plane (0.17 ± 0.1 Å) than for other pentacoordinate Fe hemeproteins (44). It has been suggested that the absence of a substantial change in CO binding for the erythrocruorin in going from pH 7 to pH 2.7 could be due to the presence of a near in-plane iron throughout this range of pH values (6). The erythrocruorin results suggest that a pentacoordinate Fe^{2+} system can have greatly enhanced ligand binding properties if the iron is sufficiently close to the heme plane. Thus both a ruptured Fe-His bond or a significantly weakened one could account for the marked enhancement of ligand binding observed in the CO binding of Mb at pH 3.

If the protonation of N_δ at pH 3 merely weakens the Fe-His bond, then, as mentioned above, the absence of the ν(Fe-His) band in the Raman spectrum of Mb* or deoxyMb could be the result of either a decrease of the frequency to a region where the laser scattering makes detection difficult, or a decrease in resonance enhancement due to a redistribution of π electron density from the iron (or heme) to the imidazole ring. Additional mechanisms may also be operative. A weakening of the Fe-His bond and a change in the hydrogen bond at N_δ might "loosen" up the orientation of the imidazole ring and allow for a less eclipsed conformation with respect to the Fe-pyrrole nitrogen axis. It has been suggested (45) that a less eclipsed conformation yields both a relative reduction in the resonance enhancement of the ν(Fe-His) band and an enhanced binding rate. In addition, if the binding of an additional proton at N_δ creates a broad distribution of hydrogen bond strengths and hence a distribution of iron displacements, it is possible that the value of ν(Fe-His) would also be widely distributed over the frequency region between ~220 and ~160 cm^{-1} or below, thus "washing" out any distinct band structure. The broad width of the ν_4(1,356) band for Mb* at pH 3 supports the possibility of a distribution of Fe-His bond lengths and thus a distribution of ν(Fe-His) positions (16).

Quantum yield

The difficulty in photodissociating pH 3 Mb is reflected both in the high residual intensity of ν(Fe-CO) and the significant amount of ν_4(1,374) observed at 15 K. Since nanosecond flash photolysis data on pH 3 Mb reveal little, if any, rebinding on the time scale of 10 ns at 15 K (8), a significant population of pH 3 MbCO either cannot be photodissociated or recombines on a subnanosecond time scale. The decrease in the R_{db} from 1.6 at 15 K to 0.6 at 80 K (λ_{exc} = 430 nm) indicates that at 80 K, a significant fraction of Mb* rebind by 10 ns. Assuming that the integrated areas of the 1,356 cm^{-1}, $A_d(t)$, and of the 1,373 cm^{-1}, $A_b(t)$, bands are respectively proportional to the number of photodissociated, $n_d(t)$, and the number of bound, $n_b(t)$, proteins probed at a time t relative to photodissociation, the recombination kinetics can be determined. The ratio of $n_b(t)$ to $n_d(t)$ is given as:

$$R_{db}(t) = A_d(t)/A_b(t) = \sum_{db} [n_d(t)/n_b(t)] \qquad (5)$$

Σ_{db} is the ratio of resonance Raman cross-sections for the 1,356 cm^{-1} to the 1,373 cm^{-1} bands, and is assumed to be independent of time. Assuming, for the purpose of a rough calculation, that the ratio of resonance Raman cross-sections is unity for the 1,356 and 1,374 cm^{-1} bands,[3] and conservation of species, $n_b(t) + n_d(t) = 1$, then the fraction of proteins in Mb* (1,356) is 0.4 ± 0.25 at 80 K and 0.6 ± 0.25 at 15 K (the range arises from the uncertainty in resonance Raman cross-sections, which we estimate to be within a factor of 3 of unity) based on a value of 2.8 (Champion, P. M., personal communication). This ratio is not necessarily the same for pH 3 Mb, but it is a lowest order guess and a range of between 1 and 5 for the ratio of resonance Raman cross-sections at 435.7 nm for Mb* compared with MbCO at pH 3, for the 30-ps data, yields a fraction of proteins in Mb* (1,356) that is 0.54 (+0.14, −0.29) at 100 K and 0.48 (+0.15, −0.23) at 160 K. These yields are in contrast to the almost complete photolysis of pH 7 MbCO as indicated by previous researchers (5, 46, 47) and by our 80 K, 10 ns, resonance Raman data which show an R_{db} of ~9 with λ_{exc} = 430 nm, which, with the ratio of

[3] We choose the ratio of resonance Raman cross-sections to be unity at 430 nm because it is about at the isobestic point for Mb* and MbCO at pH 7.

resonance Raman cross-sections of unity, gives a quantum yield of 0.9.

Rebinding kinetics

The rebinding kinetics can also be determined using Eq. 1 and the data in Table 1. Subracting off the photolysis caused by the probe pulse, as determined by $R_{db}(-60\text{ ps})$ (Fig. 6 *c* for 100 K), the fraction of photodissociated proteins, $n(t)$, is given by:

$$n_d(t) = \frac{R_{db}(t) - R_{db}(-60\text{ ps})}{R_{db}(t) + \sum_{db}} \left[\frac{\sum_{db}}{\sum_{db} + R_{db}(-60\text{ ps})} \right]. \quad (6)$$

Fig. 7 is a plot of $n_d(t)/n_d(0^+)$ (0^+ is the overlap time) at 100 K using the value of 0.54 for $R_{db}(-60\text{ ps})$ and setting the value of Σ_{db} as 2.8 at 435.7 nm, which is the value measured for Mb at pH 7 (Champion, P. M., personal communication). The error bars in the data are the spread in $n_d(t)$ which arise from using values of Σ_{db} between 1 and 5. At 100 K, 50% of the photodissociated proteins recombine within 250 ps ± 100 ps (the uncertainty in the recombination rate is primarily due to the uncertainty in Σ_{db}, which we take to be between 1 and 5). The 160 K recombination kinetics show very little deviation from the 100 K kinetics. The rapid recombination rates which do not exhibit substantial temperature dependence are consistent with the rebinding kinetics measured via flash photolysis (8, 9).

Extrapolation to room temperature

The similarities between the cryogenic and ambient temperature resonance Raman spectra for both MbCO and deoxy Mb (or Mb*) suggest that the conclusions regarding photodissociation derived from our cryogenic studies might be extended to the solution phase at ambient temperatures. The two key differences in protein behavior at room temperatures compared with cryogenic conditions are the capacity for much larger scale protein motions and the ability to rapidly reestablish an equilibrium subsequent to a perturbation.

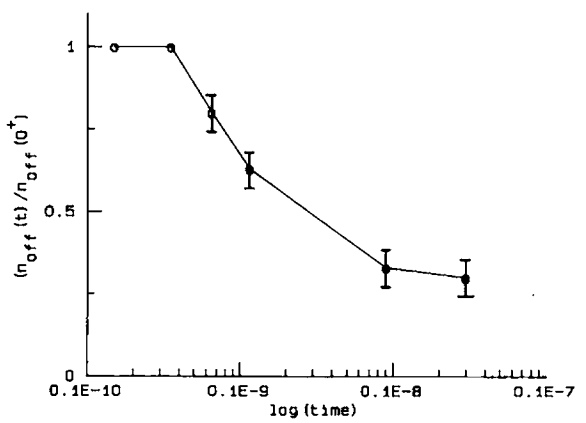

FIGURE 7 Time evolution of the number of unbound proteins, $n_d(t)$ at 100 K for photodissociated MbCO at pH 3 as determined by the resonance Raman spectra of ν_4, as seen in Fig. 6, and explained in the text.

At ambient temperatures, a solution of MbCO will contain an equilibrium mixture of protonated and unprotonated proximal environments. With a pK of 3.5, even at pH 2.5, 10% of the population remains unprotonated with respect to the proximal environment. As in our cryogenic studies, upon photodissociation, the protonated species will undergo a rupture of the Fe-His bond, and the photoproduct spectrum will primarily reflect the four-coordinate heme perturbed by the close lying protonated proximal histidine (or alternatively the perturbed pentacoordinated system discussed above). The majority of these four-coordinate (or perturbed five-coordinate) species will undergo picosecond or faster geminate recombination. From our cryogenic studies, and with analogy to other systems with picoseconds geminate rebinding rates (3, 29, 48, 49), we estimate the fraction of protonated species not undergoing geminate recombination to be no more than 0.3, and quite likely much lower.[4] Because the unprotonated photoproduct undergoes very little geminate recombination even on the nanosecond time scale (46, 47), the recombined population at early times will be derived entirely from the protonated population. Subsequent to the ultrafast geminate recombination, the MbCO population, which is now entirely protonated, will reequilibrate to the same protonated–unprotonated ratio as maintained before photolysis. Because of the reequilibration of the MbCO, repetitive or continuous excitation will drive the population toward the unprotonated photoproduct.

The unprotonated population of Mb* will now be five-coordinate, retaining the usual Fe-His bond. Because the geminate yield for MbCO with Mb* having an intact proximal linkage is only a few percent (46, 47), the unprotonated population will tend to lose the CO to the solvent. Thus, at this juncture, the MbCO population will be skewed toward the protonated species. A dispro-

[4]For a protein-ligand system, the solvent yield can be defined as the probability that a photon absorbed by the heme will break the protein-ligand bond, Γ_1, times the probability that the ligand subsequently escapes to the solvent, Γ_2. From our resonance Raman data, we estimate Γ_1 to be ~ 0.6. For protoheme, Γ_2 ~ 0.5 (3), which represents an upper linit of Γ_2, because the protein globin should decrease Γ_2 significantly. Thus, an upper limit on the solvent yield is 30%. With analogy to other systems with picosecond geminate processes, (30, 48, 49), the solvent yield may actually be significantly lower than this.

portionate fraction of the photodissociated population will therefore now be unprotonated, exhibiting an unperturbed ν(Fe-His) band. This scenario is consistent with the room temperature resonance Raman results of Sage et al. (12) on low pH Mb* photoexcited from MbCO using a C.W. laser and a rotating cell. They observe the ν(Fe-His) band with a time window of ~1–10 μs, with the time being determined by the rotation rate of the sample cell.[5]

Because recombination from the solvent is slow, (~100 μs to ~1 ms) (3, 50), the skewed unprotonated photoproduct population will reequilibrate with the solvent. The deoxy-like unprotonated photoproduct population will pick up a proton with the concomitant loss of the Fe-His linkage, thus forming the same low pH species observed on a millisecond time scale by Han and Rousseau for deoxy Mb (11) and Sage et al. for Mb* (12). This photoproduct species, which we interpret as having either a four-coordinate heme perturbed by a close lying protonated histidine, or a five-coordinate heme with a very much weakened Fe-His bond, continues to evolve as the heme ultimately moves away from the protonated proximal histidine, yielding a more typical four-coordinate heme spectrum as observed at long times (~1 s) by Sage et al. (12) for Mb*.

CONCLUSION

At cryogenic temperatures, MbCO at pH 3 has a six-coordinate, low spin heme, and relative to pH 7, the CO in an upright position due to a more open heme pocket, in agreement with the 300 K structure (11). This change in Fe-CO orientation has been associated with a protonation having a pK between ~3.8 (23) and ~4.4 (24), and has been interpreted as resulting from the protonation of the distal histidine (E7). This protonation results in an increase in the average CO rebinding rate by a factor of ~3 at 300 and 100 K (50). This protonation does not account for either the almost five orders of magnitude increase in the rebinding rate at ~100 K or the dramatic decrease in quantum yield in going from above pH 4 to pH 3 and below (5, 8, 9, 50).

Instead, we attribute these changes to proximal effects associated with the protonation of the proximal histidine. The enhanced reactivity at pH 3 and below can be understood in terms of ligand binding to a heme with a more planar iron configuration than exists for most pentacoordinate Fe^{2+} heme proteins. The reduced displacement of the iron from the heme plane can arise from either of two models which are consistent with the spectra. One possibility is that upon photodissociation, the protonated six-coordinate heme-histidine unit undergoes a rapid rupture of the Fe-His bond, resulting in a four-coordinate heme that is perturbed by the close proximity of the protonated imidazole. The other possibility is that the photoproduct remains pentacoordinate, but the added proton on N_δ results in a weakening and lengthening of the Fe-His bond. The lengthening of the bond without a shift of the histidine position would result in a diminished displacement of the iron from the heme plane. For either scenerio, the results are consistent both with the iron displacement being controlled by the protein structure and with the iron displacement being an important element in the control of ligand binding.

We wish to thank Dr. Dennis Rousseau of AT&T Bell Laboratories, Murray Hill, NJ for his advice and many helpful discussions.

Received for publication 18 June 1990 and in final form 21 December 1990.

[5]For a 1-W laser at ~430 nm, ~3×10^{-11} mole · photons are emitted in 10 μs. Assuming the light is focused to a 1-mm diam beam and impinges on a 100-μM sample with a 1-mm path length, the ratio of photons to proteins is ~0.40. Thus, with these conditions, pumping is not an issue. With a pH of 2.5 and a pK of 3.5, the fraction of protonated proteins is 0.9. With a solvent yield of 0.3 for the protonated proteins and 1.0 for the unprotonated proteins, the initial mixture of protonated to unprotonated Mb* for which the CO has escaped to the solvent will be 2.7 to 1, which is a factor of ~3.3 lower than the prephotolysis mixture of protonated to unprotonated MbCO.

REFERENCES

1. Alberding, N., R. H. Austin, S. S. Chan, L. Eisenstein, H. Frauenfelder, I. C. Gunsalus, and T. M. Nordlund. 1976. Dynamics of carbon monoxide binding to protoheme. *J. Chem. Phys.* 65:4701–4711.
2. Hill, J. R., M. J. Cote, D. D. Dlott, J. F. Kauffman, J. D. McDonald, P. J. Steinbach, J. R. Berendzen, and H. Frauenfelder. 1986. Chemical reaction in a glassy matrix: dynamics of ligand binding to protoheme in glycerol/water. *In* Ultrafast Phenomena. G. R. Flemming and A. E. Siegman, editors. Springer Verlag, Berlin. 5:433–435.
3. Postlewaite, J. C., J. B. Miers, and D. D. Dlott. 1989. Ultrafast ligand rebinding to protoheme and heme octapeptide at low temperature. *J. Am. Chem. Soc.* 111:1248–1255.
4. Suslick, K. S., M. M. Fox, and T. J. Reinert. 1984. Influences on CO and O2 binding to iron(II) porphyrins. *J. Am. Chem. Soc.* 106:4522–4525.
5. Austin, R. H., K. W. Beeson, L. Eisenstein, H. Frauenfelder, and I. C. Gunsalus. 1975. Dynamics of ligand binding to myoglobin. *Biochemistry.* 14:5355–5373.
6. Coletta, M., P. Ascenzi, T. G. Traylor, and M. Brunori. 1985. Kinetics of carbon monoxide binding to monomeric hemopro-

teins. Role of the proximal histidine. *J. Biol. Chem.* 260:4151–4155.

7. Giacometti, G. M., T. G. Traylor, P. Ascenzi, M. Brunori, and E. Antonini. 1977. Reactivity of ferrous myoglobin at low pH. *J. Biol. Chem.* 252:7447–7448.
8. Cowen, B. R. 1990. Myoglobin at pH3: dynamics of myoglobin with the iron-proximal histidine bond broken. Ph.D. thesis. University of Illinois at Urbana-Champaign, Champaign, IL.
9. Cowen, B. R., D. Braunstein, H. Frauenfelder, P. J. Steinbach, and R. D. Young. 1989. Dynamics of myoglobin with proximal histidine-iron bond broken. *Biophysics J.* 55:55a (Abstr.).
10. Spiro, T. G. 1988. Resonance Raman Spectra of Heme and Metalloproteins. Biological Applications of Raman Spectroscopy. T. G. Spiro, editor. Wiley Interscience.
11. Han, S., D. L. Rousseau, G. Giacometti, and M. Brunori. 1990. Metastable intermediates in myoglobin at low pH. *PNAS.* 87:205–209.
12. Sage, J. T., D. M. Morikis, P. Li, and P. M. Champion. 1990. Structure and kinetics of myoglobin at low pH. *Bull. Am. Phys. Soc.* 35:357–358.
13. Zipp, A., and W. Kauzmann. 1973. Pressure denaturation of metmyoglobin. *Biochemistry.* 10:4217–4228.
14. Abe, M., T. Kitagawa, and Y. Kyogoku. 1978. Resonance raman spectra of octaethylporphyrinato-Ni(II) and meso-deuterated and ^{15}N substituted derivatives. II. A Norman coordinate analysis. *J. Chem. Phys.* 69:4526–4534.
15. Spiro, T. G., and J. M. Burke. 1976. Protein control of porphyrin conformation comparison of resonance raman spectra of heme proteins with mesoporphyrin IX analogues. *J. Am. Chem. Soc.* 98:5482–5489.
16. Rousseau, D. L., and J. M. Friedman. 1988. Transient and Cryogenic Studies of Photodissociated Hemoglobin and Myoglobin in Resonance Raman Spectra of Heme and Metalloproteins. Biological Applications of Raman Spectroscopy. T. G. Spiro, editor. Wiley Interscience, New York. 133–215.
17. Kitagawa, T., and J. Teraoka. 1979. The resonance Raman spectra of intermediate-spin ferrous porphyrin. *Chem. Phys. Lett.* 63:443–445.
18. Spiro, T. G., and T. C. Strekas. 1974. Resonance Raman spectra of heme proteins. Effects of oxidation and spin state. *J. Am. Chem. Soc.* 96:338–345.
20. Ansari, A., J. Berendzen, D. Braunstein, B. R. Cowen, H. Frauenfelder, M. K. Hong, I. E. T. Iben, B. J. Johnson, P. Ormos, T. B. Sauke, R. Scholl, A. Schulte, P. J. Steinbach, J. Vittitow, and R. D. Young. 1987. Rebinding and relaxation in the myoglobin pocket. *Biophys. Chem.* 26:337–355.
21. Kitagawa, T. 1988. The Heme Protein Structure and the Iron Histidine Stretching Mode in Resonance Raman Spectra of Heme and Metalloproteins. Biological Applications of Raman Spectroscopy. T. G. Spiro, editor. Wiley Interscience, New York. 97–131.
22. Yu, N.-T., and E. A. Kerr. 1988. Vibrational modes of coordinated CO, CN^-, O_2, and NO in resonance Raman spectra of heme and metalloproteins. Biological Applications of Raman Spectroscopy. T. G. Spiro, editor. Wiley Interscience, New York. 39–95.
23. Morikis, D., and P. M. Champion. 1989. Resonance Raman investigations of site-directed mutants of myoglobin: effects of distal histidine replacement. *Biochemistry.* 28:4791–4800.
24. Ramsden, J., and T. G. Spiro. 1989. Resonance Raman evidence that distal histidine protonation removes steric hindrance to upright binding of carbon monoxide by myoglobin. *Biochemistry.* 28:3125–3128.
25. Bangcharoenpaurpong, O., K. T. Schomacker, and P. M. Champion. 1984. A resonance Raman investigation of myoglobin and hemoglobin. *J. Am. Chem. Soc.* 106:5688–5698.
26. Argade, P. V., M. Sassaroli, D. L. Rousseau, T. Inubushi, M. Ikeda-Saito, and A. Lapidot. 1984. Confirmation of the assignment of the iron-histidine stretching mode in myoglobin. *J. Am. Chem. Soc.* 106:6593–6596.
27. Kitagawa, T., T. Izuka, M. Saito, and Y. Kyogoku. 1975. Resonance Raman scattering from Hemoproteins: the nature of the bond between the sixth ligand and the heme iron in ferrous low spin derivatives of hemoglobin. *Chem. Lett.* 8:849–852.
28. Perutz, M. F., J. V. Kilmartin, K. Nagai, A. Szabo, and S. R. Simon. 1976. Influences of globin structures on the state of the heme: ferrous low spin derivatives. *Biochemistry.* 15:378–387.
29. Maxwell, J. C., and W. S. Caughey. 1976. An infrared study of NO bonding to heme B and hemoglobin A. Evidence for inositol hexaphosphate induced cleavage of proximal histidine to iron bonds. *Biochemistry.* 15:388–396.
30. Petrich, J. W., C. Poyart, and J. C. Martin. 1988. Photophysics and reactivity of heme proteins: a femtosecond absorption study of hemoglobin, myoglobin, and protoheme. *Biochemistry.* 27:4049–4060.
31. Gilson, M. K., and B. H. Honig. 1986. The dielectric constant of a folded protein. *Biopolymers.* 25:2097–2119.
32. Zerner, M., M. Gouterman, and H. Kobayashi. 1966. Extended Hückel calculations on iron complexes. *Theoret. Chim. Acta.* (Berl.). 6:363–400.
33. Agmon, N., and J. J. Hopfield. 1983. CO Binding to heme proteins: a model for barrier height distributions and slow conformational changes. *J. Chem. Phys.* 79:2042–2053.
34. Warshel, A. 1977. Energy-structure correlation in metalloporphyrins and the control of oxygen binding by hemoglobin. *Proc. Natl. Acad. Sci. USA.* 74:1789–1793.
35. Takano, T. 1977. Structure of myoglobin refined at 2.02 Å resolution II. Structure of deoxymyoglobin from sperm whale. *J. Mol. Biol.* 110:569–584.
36. Phillips, S. E. V. 1980. Sturcture and refinement of oxymyoglobin at 1.6 Å resolution. *J. Mol. Biol.* 142:531–554.
37. Phillips, S. E. V. 1978. Structure of Myoglobin. *Nature (Lond.).* 273:247–248.
38. Norvell, J. C., A. C. Nunes, and B. P. Schoenborn. 1975. Neutron diffraction analysis of myoglobin: sturcture of the carbon monoxide derivative. *Science (Wash. D.C.).* 190:568–570.
39. Stein, P., M. Mitchell, and T. G. Spiro. 1980. H-Bond and deprotonation effects on the resonance Raman iron-imidazole mode in deoxyhemoglobin models: implications for hemoglobin cooperativity. *J. Am. Chem. Soc.* 102:7795–7797.
40. Spiro, T. G., G. Smulevich, and C. Su. 1990. Probing protein structure and dynamics with resonance Raman spectroscopy: cytochrome *c* peroxidase and hemoglobin. *Biochemistry.* 29:3397-4508.
41. Smulevich, G., J. M. Mauro, L. A. Fishel, A. M. English, J. Kraut, and T. G. Spiro. 1988. Heme pocket interactions in cytochrome *c* peroxidase studied by site-directed mutagenisis and resonance Raman spectroscopy. *Biochemistry.* 27:5477–5485.
42. Friedman, J. M. 1985. Structure, dynamics and reactivity in hemoglobin. *Science (Wash. D.C.).* 228:1273–1280.
43. Amiconi, G., E. Antonini, M. Brunori, H. Formanik, and R. Huber. 1972. Functional properties of native and reconstituted

hemoglobins from chironomus thummi thummi. *Eur. J. Biochem.* 31:52–58.

44. Steigmann, W., and E. Weber. 1979. Structure of erythrocruorin in different ligand states refined at 1.4 Å resolution. *J. Mol. Biol.* 127:309–338.
45. Friedman, J. M., B. F. Cambell, and R. W. Noble. 1990. A possible new control mechanism suggested by resonance Raman spectra from deep ocean fish hemoglobin. *Biophys. Chem.* 37:43–59.
46. Friedman, J. M., and K. B. Lyons. 1988. Transient Raman study of CO-haemoprotein photolysis: origin of the quantum yield. *Nature (Lond.).* 284:570–572.
47. Henry, E. R., J. H. Sommer, J. Hofrichter, and W. A. Eaton. 1983. Geminate recombination of carbon monoxide to myoglobin. *J. Mol. Biol.* 166:443–451.
48. Martin, J. L., A. Migus, C. Poyart, Y. Lecapentier, A. Antonetti, and A. Orszag. 1982. Femtosecond photodissociation and picosecond recombination of O_2 in myoglobin: a plausible explanation for the low quantum yield in MbO_2. *Biochem. Biophys. Res. Commun.* 107:803–810.
49. Jongeward, K. A., D. Magde, D. J. Taube, J. C. Marsters, T. G. Traylor, and V. S. Sharma. 1988. Picosecond and nanosecond geminate recombination of myoglobin with CO, O_2, NO, and Isocyanides. *J. Am. Chem. Soc.* 110:380–387.
50. Doster, W., D. Beece, S. F. Bowne, E. E. Dilorio, L. Eisenstein, H. Frauenfelder, L. Reinisch, E. Shyamsunder, K. H. Winterhalter, and K. T. Yue. 1982. Control and pH dependence of ligand binding to heme proteins. *J. Biochem.* 21:4831–4839.